CBPF - CENTRO BRASILEIRO DE PESQUISAS FÍSICAS
Rio de Janeiro

Notas Técnicas

CBPF-NT-006/16
January 2017

Mediatrix method for filamentation of objects in images

C.R. Bom , M. Makler e Marcelo P. de Albuquerque

GOVERNO FEDERAL
BRASIL
PÁTRIA EDUCADORA

dx.doi.org/10.7437/NT2236-7640/2016.02.006
Notas Técnicas, v. 6, n. 2, p. 11–17, 2016

Mediatrix method for filamentation of objects in images

Método Mediatrix para filamentação de objetos em imagens

C.R. Bom*

Centro Federal de Educação Tecnológica Celso Suckow da Fonseca

Rodovia Mário Covas, lote J2, quadra J - 23810-000 Distrito Industrial de Itaguaí, Itaguaí, RJ e

Centro Brasileiro de Pesquisas Físicas, Rua Dr. Xavier Sigaud 150, Rio de Janeiro, RJ - 22290-180, Brasil

M. Makler†

Centro Brasileiro de Pesquisas Físicas, Rua Dr. Xavier Sigaud 150, Rio de Janeiro, RJ - 22290-180, Brasil

Marcelo P. de Albuquerque‡

Centro Brasileiro de Pesquisas Físicas,

Rua Dr. Xavier Sigaud 150,

Rio de Janeiro, RJ - 22290-180, Brasil

Submetido em 06/10/16 *Aceito: 23/12/16*

Resumo: Nesta contribuição, nós descrevemos o método Mediatrix para filamentação de objetos. Este método é um processo iterativo que decompõe formas em filamentos seguindo a direção do maior brilho próximo ao eixo principal utilizando mediatrizes. A partir deste método é possível obter diversos atributos morfológicos como, por exemplo, o comprimento ao longo da direção principal, largura do objeto e, no caso de objetos curvos, é possível estimar o seu centro de curvatura e seu raio de curvatura. Como um exemplo ilustrativo, nós aplicamos esta técnica em objetos com forma de arco, obtidos através de simulações de arcos gravitacionais.

Palavras chave: Processamento de Imagens, Extração de Atributos, Algoritmos.

Abstract: We describe the Mediatrix filamentation method, an iterative procedure that decomposes image shapes in filaments over their intensity ridgeline along their main direction using perpendicular bisectors. From this decomposition several morphological features can be derived, such as the length along the main direction and thickness of the object and, for curved objects, estimates of its center of curvature and curvature radius. As an example, we apply this technique to arc-shaped objects: simulated gravitational arcs.

Keywords: Image Processing, Feature Extraction, Algorithms.

1. INTRODUCTION

A reliable and robust set of characteristic features for object analysis is a recurrent issue in image processing. For example, the definition of basic morphological features, such as the length L and width W of an object, is useful in many applications and may have multiple definitions, which may be useful in different contexts.

*Electronic address: debom@cbpf.br
†Electronic address: martin@cbpf.br
‡Electronic address: marcelo@cbpf.br

In the case of curved shapes, one may also define a curvature center and radius. In this work we describe a technique to decompose shapes (images of objects) into a set of filaments to extract features such as the length L and width W and determine a curvature center. The method is well suited for curved shapes, though it is applicable to more generic shapes.

A good example of such curved shapes in an astronomical setting is given by gravitational arcs. These objects are a particular case of the Strong Lensing effect [1–3], which occurs when a distant source in the Universe (typically a galaxy), an intervening mass distribution (a galaxy or galaxy cluster) and the observer are closely aligned. This matter distribution curves the space-time, acting as a lens. Gravitational arcs are useful tools to unveil the matter distribution of galaxies and galaxy clusters (e.g. [4, 5]) and the cosmological model (e.g. [6–8]). Since they are very rare objects, several imaging surveys have been carried out on the celestial sphere to find such gravitational arc systems (e.g., [9–15]) and also in an automated fashion [12, 16–19]. The development of tools to extract features for arc-like objects, such as those derived from the method presented here, is also an important step in developing arcfinders [20, 21].

In this paper we describe the Mediatrix Filamentation method (Section 2) and a few morphological features derived from it (Section 3). We present a concrete example of application on the images of three simulated arcs (Section 4). Finally we discuss possible generalisations and other applications of the method (section 5).

2. MEDIATRIX FILAMENTATION METHOD

The method consists in decomposing objects into a set of line segments that follow its ridgeline, which may be used to determine the object "spine". For the purposes of this work we will consider pixelated objects, though the method may be applied to a more general object, not necessarily to a digital image. The only strong requirement is that the object should have a well defined boundary, i.e., it must be separated from the background.

The Mediatrix method was designed to characterize arc-like objects. Its key idea is inspired on a basic geometrical property of the perpendicular bisector of pairs of points on a circle, namely that these lines, for any set of pairs of points, intersect at the circle center. Therefore if an elongated object can be decomposed into a set of points along its longer direction, and if this object has a shape close to an arc segment, the perpendicular bisectors of pairs of these points should intersect close to the center of curvature.

The procedure to filament the object is to recursively obtain the perpendicular bisector of pairs of points on the image. For two points $P_1 = (x_1, y_1)$ and $P_2 = (x_2, y_2)$, the perpendicular bisector is a straight line $y = mx + b$ perpendicular to the segment $\overline{P_1P_2}$, intersecting this segment in its mid point and whose coefficients are given by:

$$m = -\frac{x_2 - x_1}{y_2 - y_1}, \tag{1}$$

$$b = \frac{(y_1 + y_2) - m(x_1 + x_2)}{2}. \tag{2}$$

The Mediatrix method works in n iteration steps. Each step is a new Mediatrix level. In the following, we describe the first few levels as an example.

In the first step we determine the extreme points, E_1 and E_2 of the object (i.e. the two points most distant from each other). Several methods have been considered to determine the extreme points of an object (see, e.g., [22]). Here we use the "farthest-of-farthest" method, by which E_1 is defined as the most distant point from a reference point on the object (e.g., the brightest pixel on the image or its geometrical center), whereas E_2 is defined as the pixel on the object farthest from E_1. After that, we evaluate the first perpendicular bisector between these two points. The first *Mediatrix point* M^1 is defined as the brightest pixel of the object along the perpendicular bisector. Since the object is a set of pixels, we take the brightest pixel located at a distance $d \leq \alpha\Delta p$ from the perpendicular bisector, where Δp is the pixel scale and α is chosen as $\alpha = \frac{\sqrt{2}}{2}$. The first Mediatrix Point M^1 is shown in Fig. 1(A) for an arc-shaped object (more specifically, an ArcEllipse [23]).

In the second step the perpendicular bisector is now calculated with respect to E_1, M^1 and M^1, E_2. These two perpendicular bisectors now define the next two Mediatrix Points: M_1^2 and M_2^2 using the same criteria we used to define M^1 (Fig 1B). The upper index refers to the iteration level and the lower index is a label to identify the points. Moving forward to the third step, presented in Fig 1(C), we start from the previous set of Mediatrix Points M^1, M_1^2, M_2^2 and the two extrema E_1 and E_2. Those points are used to define new Mediatrix Points in the third level M_i^3 are calculated by picking the highest intensity pixel close to the perpendicular bisector between two neighboring points of the previous iteration level. The algorithm continues defining new Mediatrix Points M_i^j, corresponding to the i-est point in the j-est iteration level, in higher iteration levels until reaching a specified final step n. In Fig 1(D), we present the last step for $n = 3$ (as in the previous panels some points were omitted not to crowd the figure). The collection of Mediatrix Points together with the two extrema are then named *keydots*. From the keydots, the object is decomposed into $N = 2^n$ segments or filaments. Each segment connects a keydot to its neighbors. The algorithm outputs a set of vectors $\vec{n}_j$, where j varies from 1 to N. Those vectors are perpendicular to the segment

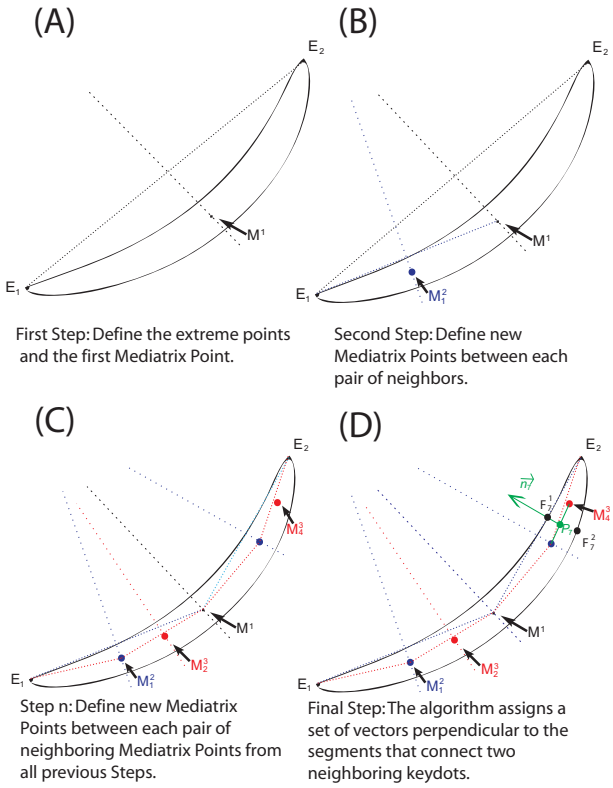

FIG. 1: Steps in the Mediatrix Filamentation method. After n iterations, the method determines a set of 2^n points defined by the maximum of intensity along the 2^n perpendicular bisectors and 2^n vectors perpendicular to neighbouring points with magnitude given by the distance between these points. For clarity, only some points are shown on the figure, which illustrates the steps for $n = 3$.

that connects a keydot to its neighbor with origin in the midpoint of this segment and norm equal to the length of the segment. This is shown in Fig. 1(D) for $\vec{n}_7$, where $|\vec{n}_7|=|\overline{M_4^3 M_2^2}|$.

3. FEATURES OBTAINED FROM THE MEDIATRIX METHOD

Using the outputs of the Mediatrix filamentation method, the object length, L, is defined as:

$$L = \sum_{j=1}^{N} |\vec{n}_j|. \tag{3}$$

The points $\vec{F}_j^1$ and $\vec{F}_j^2$, represented in Fig. 1(D) for $j = 7$, are defined as the two most distant points from the set of pixels along the perpendicular bisector associated to $\vec{n}_j$. Using those points, it is possible to estimate the average thickness W:

$$W = \frac{1}{N} \sum_{j=1}^{N} |\vec{F}_j^1 - \vec{F}_j^2|. \tag{4}$$

For arcs constructed from circle segments (as in the case of the ArcEllipse shape [23]), all perpendicular bisectors intercept at the center of curvature. Therefore, we may define as the object center of curvature the average of the points $C_{ik} = (x_{ik}, y_{ik})$ defined by the intersection of the lines in the $\vec{n}_i$ and $\vec{n}_k$ directions. The center coodinates $C_a = (x_a, y_a)$ are thus given by:

$$x_a = \frac{(N-2)!}{N!} \sum_{i=1}^{N} \sum_{k \neq i}^{N} x_{ik} \tag{5}$$

$$y_a = \frac{(N-2)!}{N!} \sum_{i=1}^{N} \sum_{k \neq i}^{N} y_{ik} \tag{6}$$

An alternative way to define a curvature center is by using the median intercept point $C_m = (x_m, y_m)$, where x_m is defined as the median of the values of x_{ik} and y_m is given by the median of y_{ik}.

From these two "center of curvature" definitions we may assign a curvature radius R_a and R_m, associated to C_m and C_a, as the distance from the first Mediatrix filamentation point M^1 to C_m or C_a respectively, i.e., $R_a = |\overline{M^1 C_a}|$ and $R_m = |\overline{M^1 C_m}|$.

4. EXAMPLE OF APPLICATION: SIMULATED GRAVITATIONAL ARCS

As an example of application of the Mediatrix filamentation method, we consider 3 arc-shaped objects produced through the gravitational lensing effect (see Fig. 2). These arcs were generated using the *AddArcs* [24] pipeline to simulate gravitational arcs.

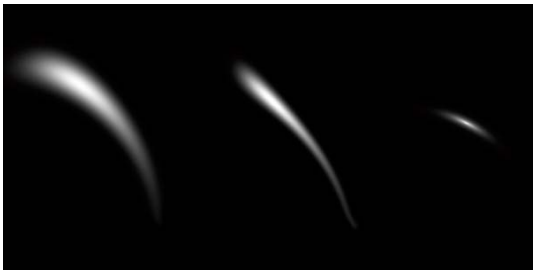

FIG. 2: Arcs A, B, and C respectively used as input for the Mediatrix method in the examples of this paper.

AddArcs is a code that simulates the surface brightness distribution of gravitational arcs, e.g., high elongated lensed objects, using the galaxy cluster abundance

(i.e. the lenses) provided by cosmological simulations and background galaxies (the sources) with morphological parameters and redshift distribution obtained from the Hubble Ultra Deep Field Survey [25, 26]. The source brightness distribution is modelled by Sérsic profiles [27] (which in principle extend to infinity) with elliptical isophotes. The lens model is given by a Navarro-Frenk-White density profile (NFW, [28, 29]), with elliptical projected density (see, e.g., [30]). Given the input models for the source and the lens, *AddArcs* controls the software *gravlens* [31] to perform the gravitational lensing calculations, resulting in one or more images of the source. The identification of individual images and their segmentation (i.e. the determination of the image pixels) is carried out using the *SExtractor* [32] software, in a similar way as to the one described in [23].

In Fig. 3 we show the results of the Mediatrix method for $n = 2$ on the 3 example objects mentioned above. The keydots are shown as black lozenge on the objects. We also show the lines spanned by the vectors $\vec{n}_i$ — perpendicular to the lines connecting neighbouring keydots — and their intersections, the points (x_{ik}, y_{ik}), as cyan lozenge. In order to avoid lines that do not intercept or are almost parallel to each other, the algorithm ignores combinations of $\vec{n}_i$ and $\vec{n}_k$ that are closely aligned, more specifically, we discard pairs with $|\tan\theta_i - \tan\theta_k| \leq 10^{-3}$, where θ_i and θ_k are the angles determined by $\vec{n}_i$ and $\vec{n}_k$ with respect to the x axis. From (x_{ik}, y_{ik}) we define the mean and median center of curvature, C_a and C_m, respectively, as described in the preceding section.

The center of the mass distribution that generated the lensing effect, the lens center $C_l = (x_l, y_l)$ is given by *AddArcs*. We define the arc radius R as the distance from the first Mediatrix filamentation point M^1 to C_l, i.e., $R = |\overline{M^1 C_l}|$. From gravitational lensing theory it is known that the curvature center of the arcs and the center of mass do not need to coincide, however, for models as the ones used in *AddArcs* (elliptical lenses), they are usually close. Therefore, we expect the fractional differences $\Delta R_m/R$ and $\Delta R_a/R$, where ΔR_m (ΔR_a) is the distance between C_l and C_m (C_a), to be small for the example objects in consideration.

In table I we show the results for some of the Mediatrix based measurements on the 3 example arcs as a function of $N = 2^n$ for up to 5 iterations of the Mediatrix filamentation. Although the results are not statistically meaningful, the behavior is representative of what we see for a large number of simulated arcs. The determination of both L and W is robust, in the sense that these quantities are weakly dependent on n and $n = 2$ already provides good estimates for them. As expected L increases with n, while W should be more stable, such that L/W has a (weak) increase with n.[1]

On the other hand the determination of the curvature center is not robust and has a strong variation with n, having an oscillatory behavior that does not seem to converge. However, the fractional difference between the lens and the arc curvature centers is minimised for $n = 2$ and $n = 3$. For these values of n, the estimates using the median are better than those using the mean. We defer to another paper a more complete and systematic analysis of the morphological properties of the objects for various shapes and iteration levels.

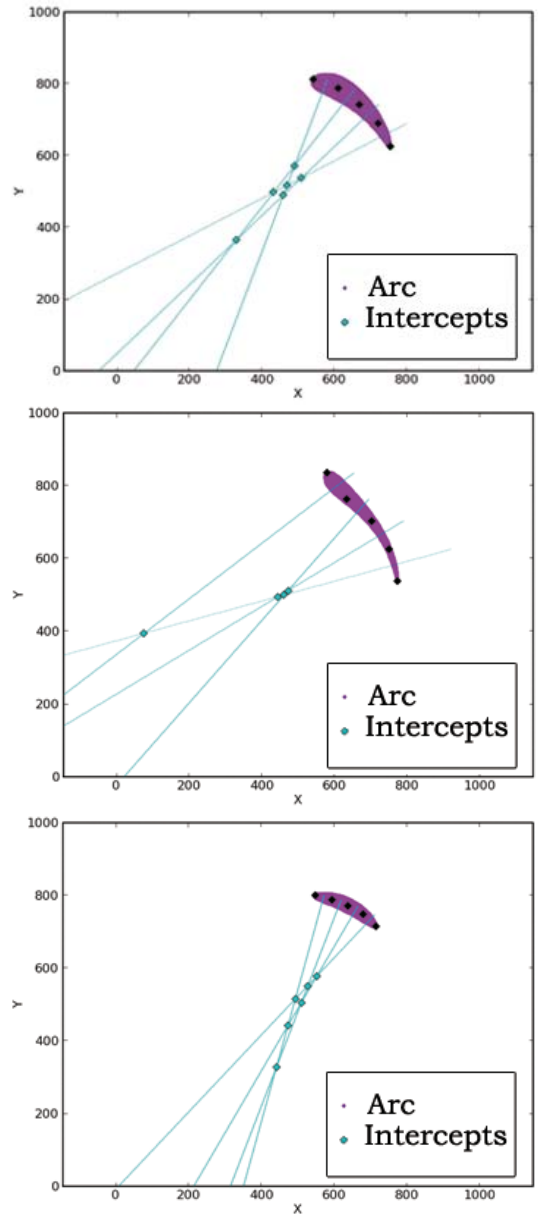

FIG. 3: Keydots (black lozenges), lines defined by the vectors $\vec{n}_j$ (cyan lines), and their intercepts (cyan lozenge), for $n = 2$. From top to bottom: arcs A, B and C.

[1] This is what we expect for images without noise and where the object L/W is large enough so that many iterations can be done without loss of information.

N	$\frac{\Delta R_m}{R}$	$\frac{\Delta R_a}{R}$	L(pixels)	L/W
Arc A				
4	0.036	0.062	294.7	5.6
8	0.153	0.126	295.3	5.6
16	0.144	0.092	295.7	5.6
32	1.09	0.230	296.8	5.7
Arc B				
4	0.100	0.096	362.4	12.6
8	0.211	0.68	363.1	12.7
16	0.166	0.170	363.3	12.7
32	0.307	0.168	363.9	12.7
Arc C				
4	0.101	0.097	192.9	5.5
8	0.051	0.093	193.1	5.5
16	0.085	0.126	193.5	5.6
32	0.198	0.209	194.7	5.6

TABLE I: Results of Mediatrix measurements for 3 simulated arcs A, B and C. The first column is the number of segments the arc was divided into. The second and third are the ratio between the distance from the lens center to the center of curvature — calculated using the average ΔR_a and median ΔR_m respectively — and the curvature radius R. The fourth column is the arc length and the fifth is the L/W ratio.

5. CONCLUDING REMARKS

The Mediatrix filamentation method is a technique to decompose elongated shapes into filaments in the main object direction, defining a "spine", which allows one to define a number of morphological features, including the length, width, and curvature center and radius. It may be used in the detection of shapes such as gravitational arcs and to provide a more generic and robust characterization of these objects.[2] For example, in ref. [23] the Mediatrix output is used to set some parameters in a method that fits the brightness distribution of gravitational arcs using analytical templates to derive their structural parameters. Another application is to use parameters derived from the Mediatrix decomposition as inputs for a neural network trained to find gravitational arcs [20, 21].

In the examples of this paper, we considered elongated objects with a well defined "main direction", a surface brightness distribution with a clear "spine", and noise-free images. However, the method can be extended to more general situations. For example, instead of using the object extrema as the first Mediatrix step, other definitions for the first step can be used for objects without a clear single preferred direction, such as objects with several tips. In this case, each pair of tips will define a different set of Mediatrix filaments and the final filamentation can be constructed as the combination of them. For binary images, where the pixels have all the same value, the midpoint of the pixels along the perpendicular bisector (i.e. the midpoint of F_j^1 and F_j^2 in figure 1) can be chosen as Mediatrix points, instead of the brightest pixel along this line.

In situations where the fluctuations on the pixel values are significant — which is often the case in astronomical images, in particular of gravitational arcs — the determination of the brightest pixel will strongly depend on the noise. In this case it is necessary to first smooth the brightness distribution using either using Gaussian isotropic kernels [32] or more sophisticated schemes, such as anisotropic smoothing [19]. In addition, in practice the filamentation procedure cannot be applied to arbitrarily large orders n. In particular, we expect to loose directional information when each segment of size $|\vec{n}_i|$ is of the order of the width $|\vec{F}_j^1 - \vec{F}_j^2|$. The criteria to stop iterating will also depend on the noise level and on the smoothing scale. A global value of n may be set or otherwise the number of iterations may be determined adaptively, at the level of each segment after a given Mediatrix step (thus choosing if that segment will be further decomposed by a new perpendicular bisector or not).

A more complete and systematic analysis will be carried out in a separate work, using a large number of real and simulated arcs (with noise, background, etc.) to determine the optimal settings for convergence and robustness of the results [34]. Extensions to other shapes will also be further investigated. However, the main aim of this paper is to present the Mediatrix filamentation method, describing its basic procedures and a few derived morphological quantities, showing an example of application to simple shapes derived by simulating the strong gravitational lensing effect leading to arcs.

ACKNOWLEDGMENTS:

C. R. Bom would like to thank CNPq for the financial support. M. Makler is partially supported by CNPq (grant 312353/2015-4) and FAPERJ (grant E-26/110.516/2012 and E-26/210.725/2015). We thank Bruno Rosseto for reminding us of the geometrical proprieties of the perpendicular bisector in a circle and Anupreeta More and Bruno Moraes for useful suggestions to the manuscript.

[1] Schneider, P, Elhers, J, Falco, EE, 1992. Gravitational lenses. Springer-Verlag, Berlin.

[2] Mollerach, S, Roulet, E, 2002. Gravitational Lensing and Microlensing, World Scientific, Singapore.

[3] Petters, AO, Levine, H, Wambsganss, J, 2001. Singularity Theory and Gravitational Lensing. Birkhäuser, Boston.

[4] Coe, D, Benítez, N, Broadhurst, T, Moustakas, LA,

2010. A High-resolution Mass Map of Galaxy Cluster Substructure: LensPerfect Analysis of A1689, Astrophys. J. 723: 1678.

[5] Carrasco, ER, Gomez, PL, Verdugo, T, Lee, H, Diaz, R, Bergmann, M, Turner, JEH, Miller, BW, West, MJ, 2010. Strong Gravitational Lensing by the Supermassive cD Galaxy in Abell 3827, Astrophys. J. Letters 715: 160.

[6] Jullo, E, Natarajan, P, Kneib, J-P, D'Aloisio, A, Limousin, M, Richard, J, Schimd, C, 2010. Cosmological Constraints from Strong Gravitational Lensing in Clusters of Galaxies, Science 329: 924.

[7] Meneghetti, M, Jain, B, Bartelmann, M, Dolag, K, 2005. Constraints on dark energy models from galaxy clusters with multiple arcs, Mon. Not. Royal Astron. Soc. 362: 1301.

[8] Yamamoto, K, Kadoya, Y, Murata, T, Futamase, T, 2001. Feasibility of Probing Dark Energy with Strong Gravitational Lensing Systems —Fisher-Matrix Approach—, Progress of Theoretical Physics 106: 917.

[9] Furlanetto, C, Santiago, BX, Makler, M, Cypriano, ES, Caminha, GB, Pereira, MES, Neto, AF, Estrada, J, Lin, H, Hao, J, McKay, TA, da Costa, LN, Maia, MAG, 2013. The SOAR Gravitational Arc Survey - I. Survey overview and photometric catalogues, Mon. Not. Royal Astron. Soc. 432: 73.

[10] Nord, B. *et al.* [DES Collaboration], [arXiv:1512.03062 [astro-ph.CO]].

[11] Bayliss, MB, 2012. Broadband Photometry of 105 Giant Arcs: Redshift Constraints and Implications for Giant Arc Statistics, Astrophys. J. 744: 156.

[12] More A, Cabanac R, More S, Alard C, Limousin M, Kneib J-P, Gavazzi R, Motta V, 2012. The CFHTLS-Strong Lensing Legacy Survey (SL2S): Investigating the Group-scale Lenses with the SARCS Sample, Astrophys. J. 749: 38.

[13] Estrada, J, Annis, J, Diehl, HT, Hall, PB, Las, T, Lin, H, Makler, M, Merritt, KW, Scarpine, V, Allam, S, Tucker, D, 2007. A Systematic Search for High Surface Brightness Giant Arcs in a Sloan Digital Sky Survey Cluster Sample, Astrophys. J. 660: 1176.

[14] Smith, GP, Kneib, J-P, Smail, I, Mazzotta, P, Ebeling, H, Czoske, O, 2005. A Hubble Space Telescope lensing survey of X-ray luminous galaxy clusters - IV. Mass, structure and thermodynamics of cluster cores at z= 0.2, Mon. Not. Royal Astron. Soc. 359: 417.

[15] Zaritsky, D, Gonzalez, AH, 2003. On the Incidence of Strong Gravitational Lensing by Clusters in the Las Campanas Distant Cluster Survey, Astrophys. J. 584: 691.

[16] Horesh, A, Maoz, D, Ebeling, H, Seidel, G, Bartelmann, M, 2012. The lensing efficiencies of MACS X-ray-selected versus RCS optically selected galaxy clusters, Mon. Not. Royal Astron. Soc. 406.

[17] Seidel, G, Bartelmann, M, 2007. Arcfinder: an algorithm for the automatic detection of gravitational arcs, Astron. & Astrophys. 472: 341-352.

[18] Alard, C, 2006. Automated Detection of Gravitational Arcs, astro-ph/0606757.

[19] Lenzen, F, Schindler, S, Scherzer, O, 2004. Automatic detection of arcs and arclets formed by gravitational lensing, Astron. & Astrophys. 416: 391L.

[20] De Bom, CR, Furlanetto, C, More, A, Brandt, C, Makler, M, Santiago, B, 2015. Finding Gravitational Arcs in Wide-Field Surveys: the Mediatrix Arcfinder and Comparison to Other Methods in a Simulated Sample, in The Thirteenth Marcel Grossmann Meeting: On Recent Developments in Theoretical and Experimental General Relativity, Astrophysics and Relativistic Field Theories: 2088.

[21] Bom, CR, Makler, M, Albuquerque, MP, Brandt, CH, A Neural Network Gravitational Arc Finder Based on the Mediatrix Filamentation Method. arXiv:1607.04644 [astro-ph.CO].

[22] Brandt, CH, Bom, CR, Ferreira, PC, Makler, M. A comparison among methods to determine image extremities: python implementation, in preparation.

[23] Furlanetto, C, Santiago, BX, Makler, M, Bom, CR, Brandt, CH et al., 2013. A simple prescription for simulating and characterizing gravitational arcs, Astron. & Astrophys. 549: A80.

[24] Brandt, CH, Dúmet-Montoya, H, Ferreira, PC, Makler, M, Neto, AF, et al. AddArcs: software for gravitational arc simulations, in preparation.

[25] Beckwith, SVW, et al., 2006. The Hubble Ultra Deep Field, The Astronomical Journal 132: 1729.

[26] Coe, D, Benítez, N, Sánchez, SF, Jee, M, Bouwens, R, Ford, H, 2006. Galaxies in the Hubble Ultra Deep Field.

I. Detection, Multiband Photometry, Photometric Redshifts, and Morphology, The Astronomical Journal 132: 926.

[27] Sérsic, JL, 1968. Atlas de Galaxias Australes, Cordoba, Argentina: Observatório Astronómico.

[28] Navarro, JF, Frenk, CS, White, SDM, 1996. The Structure of Cold Dark Matter Halos, Astrophys. J. 462: 563.

[29] Navarro, JF, Frenk, CS, White, SDM, 1997. A Universal Density Profile from Hierarchical Clustering, Astrophys. J. 490: 493.

[30] Caminha, GB, Estrada, J, Makler, M, 2013. Magnification Bias in Gravitational Arc Statistics, submitted to Astrophys. J.

[31] Keeton, CR, 2001. Computational Methods for Gravitational Lensing, astro-ph/0102340.

[32] Bertin, E, Arnouts, S. 1996. SExtractor: Software for source extraction, Astronomy and Astrophysics Supplement 117: 393.

[33] Luppino, GA, Gioia, IM, Hammer, F, Le Fèvre, O, Annis, JA, 1999. A search for gravitational lensing in 38 X-ray selected clusters of galaxies, Astronomy and Astrophysics Supplement 136: 117.

[34] Bom, CR, Makler, M, Albuquerque, MP, Brandt, CH, Ferreira, PC, 2016. Mediatrix method for object filamentation: application to gravitational arcs, submitted to Astron. & Astrophys.

Notas Técnicas é uma publicação de trabalhos técnicos relevantes, das diferentes áreas da física e afins, e áreas interdisciplinares tais como: Química, Computação, Matemática Aplicada, Biblioteconomia, Eletrônica e Mecânica entre outras.

Cópias desta publicação podem ser obtidas diretamente na página web http://revistas.cbpf.br/index.php/nt ou por correspondência ao:

Centro Brasileiro de Pesquisas Físicas
Área de Publicações
Rua Dr. Xavier Sigaud, 150 – 4º andar
22290-180 – Rio de Janeiro, RJ
Brasil
E-mail: alinecd@cbpf.br/valeria@cbpf.br
http://portal.cbpf.br/publicacoes-do-cbpf

Notas Técnicas is a publication of relevant technical papers, from different areas of physics and related fields, and interdisciplinary areas such as Chemistry, Computer Science, Applied Mathematics, Library Science, Electronics and Mechanical Engineering among others.

Copies of these reports can be downloaded directly from the website http://notastecnicas.cbpf.br or requested by regular mail to:

Centro Brasileiro de Pesquisas Físicas
Área de Publicações
Rua Dr. Xavier Sigaud, 150 – 4º andar
22290-180 – Rio de Janeiro, RJ
Brazil
E-mail: alinecd@cbpf.br/valeria@cbpf.br
http://portal.cbpf.br/publicacoes-do-cbpf